This is an *Accepted Manuscript*, which has been through the Royal Society of Chemistry peer review process and has been accepted for publication.

Accepted Manuscripts are published online shortly after acceptance, before technical editing, formatting and proof reading. Using this free service, authors can make their results available to the community, in citable form, before we publish the edited article. We will replace this *Accepted Manuscript* with the edited and formatted *Advance Article* as soon as it is available.

You can find more information about *Accepted Manuscripts* in the **Information for Authors**.

Please note that technical editing may introduce minor changes to the text and/or graphics, which may alter content. The journal's standard **Terms & Conditions** and the **Ethical guidelines** still apply. In no event shall the Royal Society of Chemistry be held responsible for any errors or omissions in this *Accepted Manuscript* or any consequences arising from the use of any information it contains.

ARTICLE TYPE

Synthesis and structural study of a new group of trigermanates, $CaRE_2Ge_3O_{10}$ (RE = La–Yb)

Olga A. Lipina,[a] Ludmila L. Surat,[a] Alexander P. Tyutyunnik,[a] Ivan I. Leonidov,*[a,b]
Emma G. Vovkotrub[c] and Vladimir G. Zubkov[a]

A new series of germanates $CaRE_2Ge_3O_{10}$ (RE = Y, La–Yb) has been prepared using an EDTA-assisted
route. Rietveld refinement of room temperature powder X-ray diffraction patterns shows that these
compounds crystallize in the monoclinic system (S.G. $P2_1/c$, Z = 4) and have two morphotropic
10 transitions. The calcium and rare earth atoms are distributed among three nonequivalent sites and form
layers along the [0 0 1] direction connected into a framework through [Ge_3O_{10}]. The morphotropic
transitions are accompanied by changes in the site occupancy factors of metal cations and by variation in
the first and second coordination spheres of Ca^{2+}/RE^{3+}.

Introduction

15 Lanthanide-doped silicates have been attracting much attention
for more than 40 years as efficient luminescent materials for
solid-state lighting because of their rigid crystal structures,
superior thermal stability, excellent optical properties and
structural diversity, which can generate plenty of local crystal
20 environments imposed on emission centers.[1, 2] Silicate optical
hosts doped with lanthanide Ln^{n+} (n = 2, 3) ions convert either
high energy radiation or ultraviolet to visible light and are used as
fluoroscopic screens, plasma display panels, fluorescent lamps,
white light-emitting diodes (LEDs), scintillators, etc.[3] A number
25 of basic and important optical hosts for inorganic luminescent
materials belong to the systems $M^{II}O$–Y_2O_3–SiO_2 (M = Ca, Sr,
Ba).[4, 5] The luminescence properties of $Ca_3Y_2(SiO_4)_3$,[6, 7]
$Ca_2Y_2Si_2O_9$,[8] $Ca_4Y_6(SiO_4)_6O$,[9] $M_2Y_8(SiO_4)_6O_2$ (M = Ca, Sr)[10] and
$M_3Y_2(Si_3O_9)_2$ (M = Ca, Sr)[11] doped with lanthanide ions have
30 been discussed in numerous previous papers. The energy transfer
processes $Ce^{3+} \rightarrow Tb^{3+}$ in $M_3Y_2(Si_3O_9)_2$:Ce^{3+},Tb^{3+} (M = Ca, Sr)
and $Ce^{3+} \rightarrow Mn^{2+}$ in $Ca_3Y_2(Si_3O_9)_2$:Ce^{3+},Mn^{2+} have been reported
by several groups.[12] With the rapid development of white LEDs,
many Ce^{3+}/Eu^{2+}-doped and Ce^{3+},Tb^{3+}-codoped silicate
35 compounds excited by near ultraviolet or blue light have been
synthesized in recent years, such as Sr_3SiO_5:Eu^{2+}/Ce^{3+},[13]
Li_2SrSiO_4:Eu^{2+},[14] $BaZrSi_3O_9$:Eu^{2+},[15] $Na_4CaSi_3O_9$:Ce^{3+16} and
$A^+B^{2+}ScSi_2O_7$:Eu^{2+} (A = Na, K; B = Ca, Sr, Ba).[17] Some of them,
including $(Sr,Ba)_2SiO_4$:Eu^{2+18} and $Sr_3Y_2(Si_3O_9)_2$:Ce^{3+},Tb^{3+},[19]
40 demonstrate the maximum quantum yields of more than 90%
under ultraviolet excitation.

Despite the excellent host matrix properties, the silicates are
not completely free of lattice defects which may either decrease
drastically the emission intensity or lead to persistent
45 luminescence observed often in dozens of silicate phosphors, as

in the case of $CdSiO_3$:Ln^{3+} (Ln = Pr, Sm, Gd, Tb, Dy),[20, 21]
Ln_2SiO_5:Ce^{3+} (Ln = Y, Lu),[22] $M_2MgSi_2O_7$:Eu^{2+},Ln^{3+} (M = Ca, Sr,
Ba; Ln = Pr–Nd, Sm, Gd–Lu, Y)[23] whose afterglow properties
have been summarized by Van den Eeckhout, et al.[24] On the other
50 hand, fast and efficient scintillation crystals Ln_2SiO_5:Ce^{3+25},
Ln_2SiO_5:Pr^{3+26}, $Ln_2Si_2O_7$:Ce^{3+27} (Ln = Y, La, Gd, Lu) and
$Ca_3Sc_2Si_3O_{12}$:Pr^{3+},Mg^{2+28} have been extensively studied.

The $BaY_2Si_3O_{10}$ trisilicate characterized structurally by
Kolitsch et al.[29] a few years ago represents a new optical host for
55 the color tunable phosphors $BaY_2Si_3O_{10}$:Ln^{3+}, Ln = Ce, Tb, Eu)[30]
and $BaY_2Si_3O_{10}$:Ce^{3+},Tb^{3+31} showing quantum yields of up to
82%. $BaY_2Si_3O_{10}$ (S. G. $P2_1/m$, Z = 2) and its isotypic analogues
$BaRE_2Si_3O_{10}$ (RE = Gd, Er, Yb, Sc) belong to a small family of
uncommon compounds $MRE_2T_3O_{10}$, (RE = Sc, Y, Lanthanide;
60 M = Ca, Co, Sr, Ba; T = Si, Ge) whose crystal structures comprise
isolated $[T_3O_{10}]^{8-}$ (T = Si, Ge) anions.[32, 33] Meanwhile, various
oxides featuring the T_3O_{10} trimers (T = Si, Ge, P, As, Al, Ga, V)
with additional building units, such as TO_4 or T_2O_7 groups and
protonated variants are widespread.[32, 34] The trisilicates
65 $MRE_2Si_3O_{10}$ (RE = Sc, Y, Lanthanide; M = Co, Sr, Ba) contain
Si_3O_{10} units located between zigzag chains of either edge-shared
distorted LnO_6 octahedrons, or Y_2O_{11} dimers ($SrY_2Si_3O_{10}$), or
Co_2O_{10} dimers ($CoEu_2Si_3O_{10}$),[32] whereas the crystal structure of
$CaY_2Ge_3O_{10}$ (S. G. $P2_1/c$, Z = 4) features isolated tritetrahedral
70 Ge_3O_{10} groups and Ca/Y coordinated by seven oxygen atoms.[33]
The adjacent edge- and corner-shared metal-oxygen polyhedrons
are connected to the framework through Ge_3O_{10}. Unlike
$MRE_2Si_3O_{10}$ (RE = Sc, Y, Lanthanide; M = Co, Sr, Ba), where
metal cations occupy their unique sites, there are three
75 nonequivalent sites with mixed distributions of Y^{3+} and Ca^{2+} in
the $CaY_2Ge_3O_{10}$ germanate whose structural formula is expressed
as $(Ca_{0.45}Y_{0.55})(Ca_{0.46}Y_{0.54})(Ca_{0.09}Y_{0.91})Ge_3O_{10}$.[33]

Doping of the $CaY_2Ge_3O_{10}$ host with lanthanide ions allows
constructing a new promising series of phosphor-converted

LEDs.[35] Apart from the nature of the activator ions, the luminescence properties of various phosphor materials highly depend on the crystal structures of their host lattices, and understanding of the chemistry and structure plays a crucial role in phosphor preparation.[3] The difference in the crystal radii for RE^{3+} in $CaRE_2Ge_3O_{10}$, RE = Y, La–Yb, is expected to lead to essential changes in the crystal structure implying variations of Ca–RE mixed distributions and the Ge_3O_{10} geometry which, in their turn, may affect the optical properties of phosphors based on $CaM_2Ge_3O_{10}$:Ln^{3+}, M = Y, La, Lu; Ln = Ce–Yb. The aim of this work is the synthesis and structural study of a new series of germanates $CaRE_2Ge_3O_{10}$, RE = Y, La–Yb.

Experimental section

Chemicals and preparation

$CaRE_2Ge_3O_{10}$ (RE = Y, La–Yb) were prepared using an ethylenediamine tetraacetic acid (EDTA) assisted route. The appropriate amounts of RE_2O_3 (99.98%), RE = Y, La, Nd, Eu–Yb; $Pr(OH)_3$, (99.98%) and $CaCO_3$ (99.9%) were dissolved in nitric acid (1:3). The Tb_2O_3 oxide was prepared by the reduction of Tb_4O_7 in hydrogen at 1300 °C for 24 hours. A dilute solution of ammonia was used for dissolving GeO_2 (99.5%). EDTA was employed as a complexing agent taken in the mole ratio 1:1 to the total amount of cations. Ammonium hydroxide was added to enhance the dissolution of EDTA in distilled water. Three solutions were obtained: one of them contained Ca^{2+} and RE^{3+}, the second – Ge^{4+} and the third – EDTA–NH_3 solution. All the solutions were merged together, vigorously stirred at room temperature for 3 h, and heated in evaporating dishes at 90–95 °C. The resulting dark grey gels were calcined at 800–1000°C in air to remove the organic component. Then the as-prepared powders were pressed into pellets and annealed at 1100 °C for 6 h in air, or in argon in case of praseodymium and terbium samples.

Characterizations

The single-phase character of the final products was checked by X-ray powder diffraction (XRD). All XRD patterns were collected on a STOE STADI–P automated diffractometer equipped with a linear mini–PSD detector using Cu $K\alpha_1$ radiation in the 2θ range from 5° to 120° with a step of 0.02°. Polycrystalline silicon (a = 5.43075(5) Å) was used as an external standard. The phase purity of the samples was checked by comparing their XRD patterns with those in the PDF2 database (ICDD), release 2009.

The crystal structure refinements were carried out with the GSAS program suite (Figs. S1–S12 in the ESI†).[36] The peak profiles were fitted with a pseudo–Voigt function, $I(2\theta) = x*L(2\theta) + (1–x)*G(2\theta)$ (where L and G are the Lorentzian and Gaussian part, respectively). The angular dependence of the peak width was described by the relation $(FWHM)^2 = Utg^2\theta + Vtg\theta + W$, where $FWHM$ is the full line width at half maximum. The background level was described by a combination of thirty-six-order Chebyshev polynomials. The absorption correction function for a flat plate sample in transmission geometry was applied. The crystal structure of $CaY_2Ge_3O_{10}$[33] was used as a starting model for the full profile refinement of $CaRE_2Ge_3O_{10}$ (RE = Y, Pr–Yb). The structure of $CaLa_2Ge_3O_{10}$ was solved by the direct method using EXPO2013.[37] The sum of fractions of

calcium and rare earth atoms was fixed to 1.0 using Fractions Constrains, and chemical restrains were used to keep the overall composition. Density measurements were carried out on a Micromeritics AccuPyc II 1340 Gas Displacement Pycnometer with a sample chamber of 1 cm³. About 50–60 % of the chamber volume was filled with the powder samples, and 15 measurements were done for each sample.

Infrared spectroscopy was performed using the CsI pellet technique with a Bruker Vertex 80 FTIR spectrometer. The spectra obtained were the average of 64 scans over the 165–4000 cm⁻¹ range with 4 cm⁻¹ resolution. The Raman spectra were recorded on a Renishaw Raman microscope-spectrometer U1000 equipped with a confocal Leica DML microscope, 50× objective, a notch filter, and a cooled charge-coupled device detector. A Renishaw HeNe laser operating at 633 nm and 5 mW at the sample was employed as an excitation source. The typical spectra acquisition time was 600 s, and the resolution was 1 cm⁻¹. The Raman spectrum of yttrium oxide was used for spectral calibration. The spectroscopic measurements listed above were carried out at room temperature.
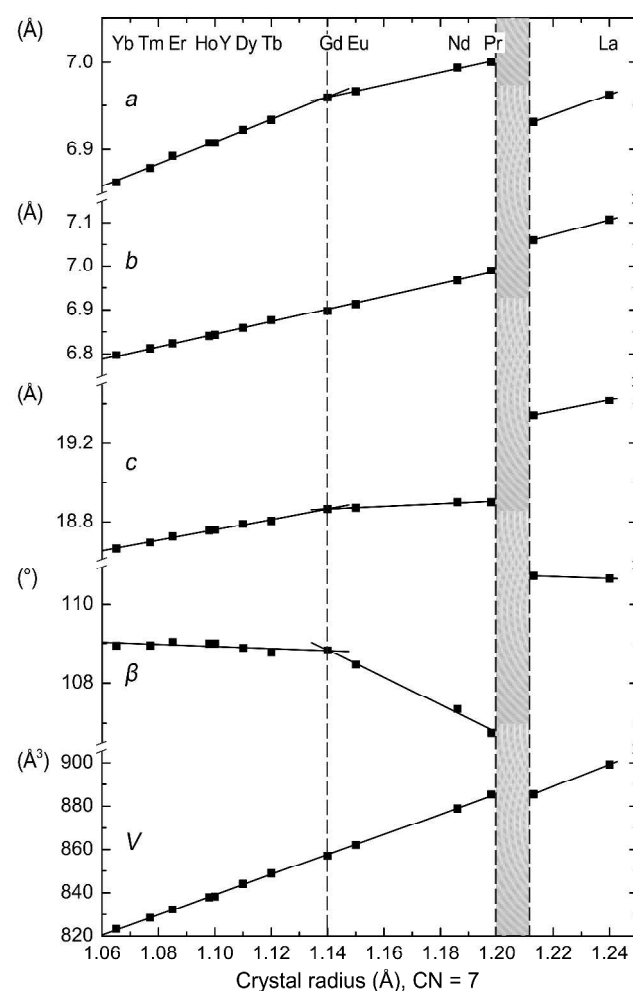

Fig. 1   The lattice parameters vs. rare earth crystal radius in seven-fold coordination[38] in the structure of $CaRE_2Ge_3O_{10}$ (RE = Y, La–Yb). Error widths do not exceed the size of the dots. The values of crystal radii in seven-fold coordination estimated as mean values of radii in six- and eight-fold coordination are taken for Pr, Nd, Ho, Tm.

Results and discussion

Crystal structure

The powder XRD patterns of $CaRE_2Ge_3O_{10}$ (RE = Y, La–Yb) have been indexed with monoclinic unit cells and the space group $P2_1/c$, Z = 4. The crystallographic data, experimental details and R-values are listed in Tables 1 and 2. The atomic coordinates, isotropic thermal parameters and Ca^{2+}–RE^{3+} fractions can be found in the ESI† (Tables S1–S4). The dependences of the lattice parameters on the rare earth ion crystal radius with sevenfold coordination (CN = 7)[38] are shown in Fig. 1.

Although all the compounds crystallize in the same space group, the unit cell volume increases linearly only from Yb to Pr, while $CaLa_2Ge_3O_{10}$ clearly deviates from this dependence, which indicates a first-order morphotropic transition.[39] Thus, the formation of a continuous solid solution between $CaRE_2Ge_3O_{10}$ (RE = Pr–Yb) and $CaLa_2Ge_3O_{10}$ is impossible because of the crystal structure differences. The $CaLa_{1.4}Eu_{0.6}Ge_3O_{10}$ germanate with an average crystal radius of 1.21 Å for Ca, La and Eu has been synthesized to determine the two-phase region. This sample consists of two phases: 93.5 mass % with the structure type of $CaLa_2Ge_3O_{10}$ and the unit cell parameters a = 6.9316(1), b = 7.0597(1), c = 19.3434(3) Å, β = 110.7023(7)°, V = 885.44(2) Å^3, and the rest 6.5 % isostructural to $CaPr_2Ge_3O_{10}$ with the lattice parameters a = 6.993(1), b = 6.964(1), c = 18.925(2) Å, β = 107.36(1)°, V = 879.7(2) Å^3. Inclusion of unit cell parameters of the main phase to the dependencies shown in Fig. 1 specifies the boundaries of the two phase region (hatched area) from average crystal radius 1.198 Å to 1.21 Å.

An accurate inspection of the unit cell parameters vs. the crystal radius of rare earth ions reveals the change in direction of the linear dependence between Gd and Eu, which is most pronounced for the parameters c and β (Tables 1 and 2; Fig. 1). These inflection points of the lattice parameters without any apparent volume change may indicate a second-order continuous morphotropic transition in this germanate family. The confirmation for this statement can be done bearing in mind an analogy with the second derivatives for Gibbs function which should be discontinuous for a second-order transition. Similarly to a thermal expansion coefficient at a polymorphic transition, a coefficient can be considered to depend on the crystal radius of rare earth ion. Dependences of an effective size of structural units or crystal radii on external factors, such as temperature and pressure can correlate with each other. Pressure reduces the lattice and should induce the structure transition $\mathbf{1}\rightarrow\mathbf{3}$, while temperature increase may lead to extension of the lattice size and should cause a polymorphic transition $\mathbf{3}\rightarrow\mathbf{1}$ that can be expressed as follows.

$$p \rightarrow$$
$$La\ \mathbf{1} \rightarrow Pr–Eu\ \mathbf{2} \rightarrow\ Gd–Yb\ \mathbf{3}$$
$$\leftarrow T$$
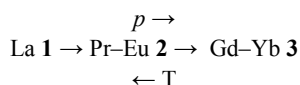
Therefore, such expansion coefficient can be written as

$$\alpha_L = \frac{1}{L}\left(\frac{\partial L}{\partial R}\right),\ \text{Å}^{-1}, \tag{1}$$

here, L – lattice parameter, R – crystal radius of rare earth. The
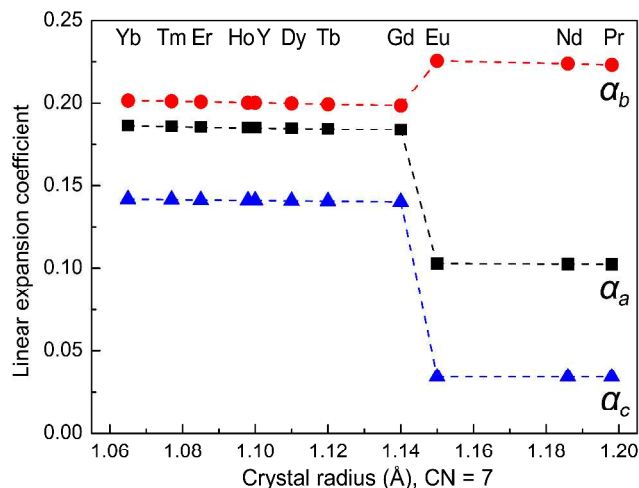
Fig. 2 The linear expansion coefficients vs. crystal radius in seven-fold coordination[38] in the structure of $CaRE_2Ge_3O_{10}$ (RE = Y, La–Yb). The values of crystal radii in seven-fold coordination estimated as mean values of radii in six- and eight-fold coordination are taken for Pr, Nd, Ho, Tm.
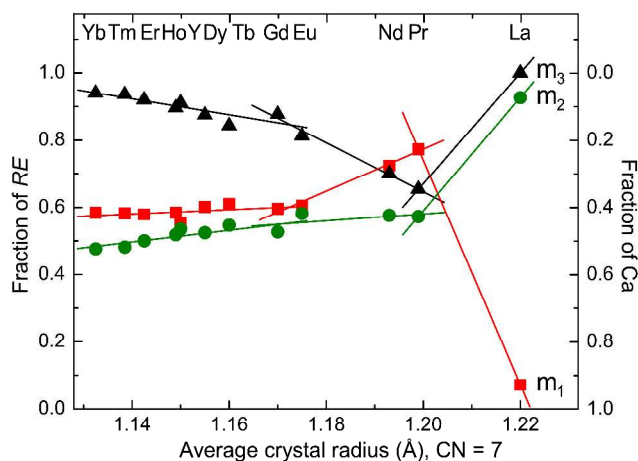
Fig. 3   The dependences of cation fractions on the average crystal radius for $CaRE_2Ge_3O_{10}$ (RE = Y, La–Yb); Ca(1)/RE(1) stands for $\mathbf{m_1}$, Ca(2)/RE(2) – $\mathbf{m_2}$ и Ca(3)/RE(3) – $\mathbf{m_3}$.
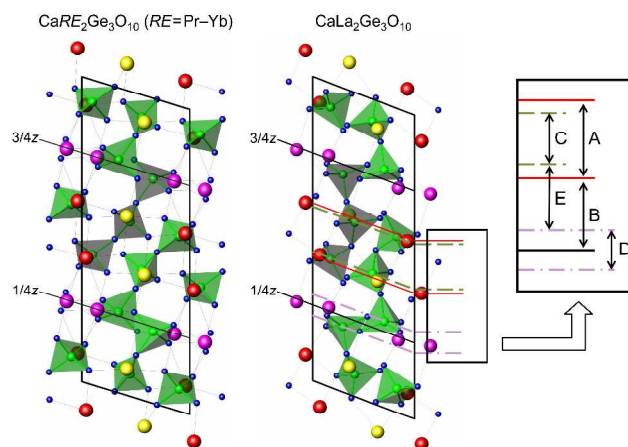
Fig. 4   The crystal structure of $CaRE_2Ge_3O_{10}$ (RE = La–Yb) and GeO_4 tetrahedrons (green), Ca(1)/RE(1) atoms (red), Ca(2)/RE(2) atoms (yellow), Ca(3)/RE(3) atoms (lilac).

Table 1 Crystallographic data and refinement parameters for $CaRE_2Ge_3O_{10}$ (RE = La–Tb)

	La	Pr[a]	Nd	Eu	Gd	Tb
a, Å	6.96261(5)	7.0001(1)	6.9938(1)	6.9668(2)	6.95931(9)	6.9337(2)
b, Å	7.10680(6)	6.9892(1)	6.9666(1)	6.9131(1)	6.89700(8)	6.8761(1)
c, Å	19.4194(1)	18.8994(3)	18.8991(3)	18.8713(4)	18.8648(2)	18.8052(4)
β, °	110.6357(4)	106.7689(8)	107.3452(8)	108.463(1)	108.8194(7)	108.766(1)
V, Å^3	899.26(1)	885.34(3)	878.95(3)	862.10(3)	857.07(2)	848.92(3)
CR[b], Å	1.24	*1.198*	*1.186*	1.15	1.14	1.12
ρ_{calc}, g/cm^3	5.108(5)	5.212(4)	5.26(1)	5.36(1)	5.638(1)	5.419(6)
ρ_x, g/cm^3	5.138	5.249	5.338	5.561	5.675	5.756
R_{wp}, %	2.02	2.36	1.66	1.05	1.01	1.28
R_p, %	1.52	1.72	1.20	0.81	0.80	1.00
χ^2	2.641	2.072	2.452	1.575	1.221	1.424
$R(F^2)$, %	2.50	4.41	4.54	3.62	4.81	2.97

[a] Content of impurity 4.8 m.% $Pr_{8.133}Ca_{1.8}(GeO_4)_6O_2$.

[b] CR stands for crystal radii in seven-fold coordination.[38] Theoretical values estimated as mean values of radii in six- and eight-fold coordination are given in *italics*.

Table 2 Crystallographic data and refinement parameters for $CaRE_2Ge_3O_{10}$ (RE = Y, Dy–Yb)

	Dy	Y	Ho	Er	Tm	Yb
a, Å	6.9227(1)	6.90763(6)	6.90770(5)	6.89238(4)	6.87838(5)	6.86205(4)
b, Å	6.8586(1)	6.84276(5)	6.84060(5)	6.82361(4)	6.81237(5)	6.79741(4)
c, Å	18.7895(4)	18.7583(2)	18.7555(2)	18.7245(1)	18.6937(1)	18.6633(1)
β, °	108.885(1)	108.9988(5)	108.9903(5)	109.0386(4)	108.9428(5)	108.9369(4)
V, Å^3	844.10(3)	838.36(1)	838.01(1)	832.457(9)	828.51(1)	823.417(9)
CR[a], Å	1.11	1.10	*1.098*	1.085	*1.077*	1.065
ρ_{calc}, g/cm^3	5.771(6)	4.609(3)	5.896(9)	5.988(6)	6.067(8)	6.11(1)
ρ_x, g/cm^3	5.845	4.719	5.926	6.003	6.058	6.162
R_{wp}, %	0.96	4.98	3.05	3.21	4.16	3.67
R_p, %	0.75	3.68	2.17	2.30	2.93	2.69
χ^2	1.472	4.000	5.292	6.075	6.218	9.291
$R(F^2)$, %	2.69	2.64	2.30	2.04	2.73	2.08

[a] CR stands for crystal radii in seven-fold coordination.[38] Theoretical values estimated as mean values of radii in six- and eight-fold coordination are given in *italics*.

derivatives have been taken from slopes of the cell dependences represented in Fig. 1. The linear expansion coefficients calculated for three directions in the unit cell demonstrate the obvious discontinuity (Fig. 2). The step-like change of linear expansion coefficients can originate from atomic displacement or an order-disorder transformation. The average crystal radius of Ca^{2+} and RE^{3+} determined as $[r(Ca^{2+}) + r(RE^{3+})]/2$ for CN = 7 can be used to analyze the specific features of the crystal structures. The dependences of the Ca^{2+}–RE^{3+} site occupancies factors (SOFs) on the average cation radius have significant variation, starting from almost fully ordered site **m₃** and disordered **m₁** and **m₂** for the Yb–Gd series. Then in the Eu–Pr compounds, the site **m₃** undergoes disorder, while **m₁** has some ordering. Finally, all the Ca^{2+}–RE^{3+} sites become completely ordered in the structure of $CaLa_2Ge_3O_{10}$ (Fig. 3). This change in the ordering could be the reason of these two morphotropic transitions. It is worth noting that the calcium and yttrium SOFs in $CaY_2Ge_3O_{10}$ calculated in our work are close to those reported by Yamane.[33]

Fig. 4 illustrates the crystal structures of $CaRE_2Ge_3O_{10}$ (RE = La–Yb) before and after the first-order morphotropic transition. In both cases, calcium and rare earth atoms form layers along the [0 0 1] direction connected into a framework through Ge_3O_{10} groups. The Ge–O bond distances in $CaRE_2Ge_3O_{10}$ are in the range from 1.584(21) to 1.867(22) Å, which are comparable to those reported for other compounds comprising Ge_3O_{10} units (1.626–1.902 Å).[33, 34] However, the main difference is related to rotation of the tritetrahedral germanate unit in $CaRE_2Ge_3O_{10}$ (RE = Pr–Yb) and $CaLa_2Ge_3O_{10}$. The $Ge(1)O_4$ tetrahedrons turn at ~5°, while rotation of $Ge(3)O_4$ is about 40°. The significant angle change of the latter results in the formation of almost eclipsed conformation with dihedral angle of ~9.6° that promotes increasing in interactions between oxygen atoms and variation of the Ge_3O_{10} geometry (Fig. 5). In the first subgroup, the Ge–Ge–Ge angle changes gradually with the crystal radius from 144.7°(Yb) to 148.4° (Pr), but in $CaLa_2Ge_3O_{10}$ it has the smallest value of 116.2° (Tables 3 and 4).

Table 3 Selected bond lengths (Å), angles (°) and specific distances (Å) for $CaRE_2Ge_3O_{10}$ (RE = La–Tb)

	La	Pr	Nd	Eu	Gd	Tb
Bond lengths						
Ca(1)/RE(1)–O(1)	2.362(11)	2.426(19)	2.404(17)	2.419(19)	2.312(17)	2.341(19)
Ca(1)/RE(1)–O(2)	2.436(10)	2.500(19)	2.464(17)	2.445(20)	2.468(17)	2.399(20)
Ca(1)/RE(1)–O(2)		2.593(23)	2.595(20)	2.596(22)	2.491(18)	2.531(20)
Ca(1)/RE(1)–O(3)		2.517(21)	2.539(19)	2.629(21)	2.419(18)	2.565(20)
Ca(1)/RE(1)–O(4)[a]		2.919(22)	3.052(20)	3.389(2)	*3.269(17)*	*3.332(19)*
The valence of the Ca(1)/RE(1)–O(4) bond[b]		*0.121*	*0.053*	*0.021*	*0.030*	*0.025*
Ca(1)/RE(1)–O(5)		2.707(22)	2.631(18)	2.690(21)	2.659(17)	2.617(19)
Ca(1)/RE(1)–O(7)	2.434(11)	2.371(19)	2.346(16)	2.254(19)	2.317(15)	2.257(17)
Ca(1)/RE(1)–O(7)	2.285(12)					
Ca(1)/RE(1)–O(8)	2.265(11)					
Ca(1)/RE(1)–O(10)	2.292(11)	2.402(20)	2.326(18)	2.247(19)	2.347(17)	2.298(17)
<Ca(1)/RE(1)–O>	**2.344**	**2.554**	**2.472**	**2.469**	**2.430**	**2.430**
Ca(2)/RE(2)–O(1)	2.411(11)					
Ca(2)/RE(2)–O(2)	2.480(10)	2.373(20)	2.394(18)	2.349(20)	2.329(19)	2.313(20)
Ca(2)/RE(2)–O(4)	2.423(9)					
Ca(2)/RE(2)–O(5)	2.430(10)	2.343(21)	2.463(19)	2.408(23)	2.420(19)	2.351(21)
Ca(2)/RE(2)–O(6)	2.807(10)	2.807(21)	2.723(20)	2.671(21)	2.590(18)	2.628(20)
Ca(2)/RE(2)–O(7)	2.510(10)	2.416(20)	2.357(18)	2.293(20)	2.321(16)	2.263(18)
Ca(2)/RE(2)–O(8)		2.446(22)	2.454(20)	2.483(22)	2.341(18)	2.444(19)
Ca(2)/RE(2)–O(9)	2.549(11)	2.530(20)	2.571(19)	2.519(20)	2.503(18)	2.485(20)
Ca(2)/RE(2)–O(10)		2.375(22)	2.404(20)	2.337(22)	2.306(19)	2.225(21)
<Ca(2)/RE(2)–O>	**2.516**	**2.470**	**2.481**	**2.437**	**2.401**	**2.387**
Ca(3)/RE(3)–O(1)		2.328(24)	2.377(21)	2.192(24)	2.312(20)	2.188(23)
Ca(3)/RE(3)–O(2)	2.743(10)					
Ca(3)/RE(3)–O(3)	2.447(11)	2.331(20)	2.382(18)	2.358(18)	2.315(15)	2.296(17)
Ca(3)/RE(3)–O(3)	2.410(1)	2.553(20)	2.510(18)	2.451(18)	2.506(16)	2.473(17)
Ca(3)/RE(3)–O(4)	2.500(9)	2.428(18)	2.282(16)	2.157(20)	2.210(15)	2.168(17)
Ca(3)/RE(3)–O(4)		2.534(20)	2.515(17)	2.551(18)	2.446(16)	2.401(18)
Ca(3)/RE(3)–O(5)	2.586(11)	2.458(21)	2.405(20)	2.320(23)	2.296(19)	2.320(20)
Ca(3)/RE(3)–O(8)	2.805(10)	2.326(22)	2.424(21)	2.387(23)	2.355(18)	2.328(20)
Ca(3)/RE(3)–O(8)	2.464(10)					
Ca(3)/RE(3)–O(10)	2.581(11)					
<Ca(3)/RE(3)–O>	**2.567**	**2.423**	**2.414**	**2.345**	**2.349**	**2.311**
Bond angles						
Ge(1)–O(6)–Ge(2)	137.4(6)	123.6(12)	120.6(11)	124.3(12)	117.6(9)	119.6(11)
Ge(2)–O(9)–Ge(3)	125.6(6)	120.7(12)	125.7(11)	125.8(11)	134.8(9)	123.0(11)
Ge(1)–Ge(2)–Ge(3)	116.9(10)	147.84(21)	148.38(17)	145.90(21)	145.37(18)	145.79(22)
Specific distances						
A, Å	3.066	3.187	3.153	3.070	3.025	3.045
B, Å	3.010	2.931	2.933	2.940	2.952	2.929
C, Å	2.751	2.615	2.630	2.671	2.619	2.644
D, Å	1.236	0.575	0.527	0.322	0.311	0.328
E, Å	2.550	2.929	2.931	2.978	2.999	2.965

[a] The values of the distances between Ca and O(4) outside the first coordination sphere are given in *italics*. The value of Ca(1)/La(1)–O(4) is more than 4.000 Å.

[b] The bond valences calculated from the data by I. D. Brown and D. Altermatt.[40] The Ca(1)/RE(1)–O(4) distances and the corresponding bond valences have been calculated from the assumption of the first site to be occupied by only RE atoms.

Table 4 Selected bond lengths (Å), angles (°) and specific distances (Å) for $CaRE_2Ge_3O_{10}$ (RE = Y, Dy–Yb)

	Dy	Y	Ho	Er	Tm	Yb
Bond lengths						
Ca(1)/RE(1)–O(1)	2.367(16)	2.364 (8)	2.323(8)	2.333(8)	2.330(10)	2.323(8)
Ca(1)/RE(1)–O(2)	2.389(17)	2.446 (8)	2.402(9)	2.411(8)	2.406(10)	2.402(8)
Ca(1)/RE(1)–O(2)	2.576(17)	2.516(8)	2.556(9)	2.524(8)	2.547(10)	2.508(9)
Ca(1)/RE(1)–O(3)	2.585(17)	2.395 (8)	2.447(8)	2.396(8)	2.411(10)	2.416(8)
Ca(1)/RE(1)–O(4)[a]	*3.391(17)*	*3.340(8)*	*3.372(9)*	*3.384(8)*	*3.368(10)*	*3.371(9)*
The valence of the Ca(1)/RE(1)–O(4) bond[b]	*0.021*	*0.024*	*0.026*	*0.023*	*0.025*	*0.022*
Ca(1)/RE(1)–O(5)	2.628(17)	2.647 (8)	2.641(9)	2.630(8)	2.622(10)	2.615(8)
Ca(1)/RE(1)–O(7)	2.269(15)	2.288 (7)	2.268(8)	2.261(7)	2.241(9)	2.220(8)
Ca(1)/RE(1)–O(7)						
Ca(1)/RE(1)–O(8)						
Ca(1)/RE(1)–O(10)	2.314(15)	2.285(8)	2.261(8)	2.269(8)	2.289(10)	2.280(8)
<Ca(1)/RE(1)–O>	**2.447**	**2.420**	**2.414**	**2.403**	**2.407**	**2.395**
Ca(2)/RE(2)–O(1)						
Ca(2)/RE(2)–O(2)	2.287(18)	2.291(8)	2.314(9)	2.318(8)	2.297(10)	2.302(8)
Ca(2)/RE(2)–O(4)						
Ca(2)/RE(2)–O(5)	2.393(19)	2.400(9)	2.382(9)	2.387(8)	2.397(11)	2.379(9)
Ca(2)/RE(2)–O(6)	2.644(18)	2.607(8)	2.620(9)	2.631(8)	2.653(10)	2.673(9)
Ca(2)/RE(2)–O(7)	2.284(15)	2.294(8)	2.297(8)	2.301(7)	2.301(10)	2.315(8)
Ca(2)/RE(2)–O(8)	2.416(17)	2.360(8)	2.356(8)	2.356(8)	2.348(10)	2.346(8)
Ca(2)/RE(2)–O(9)	2.502(17)	2.427(8)	2.467(9)	2.429(8)	2.430(10)	2.417(8)
Ca(2)/RE(2)–O(10)	2.222(18)	2.261(8)	2.250(9)	2.262(8)	2.240(10)	2.259(9)
<Ca(2)/RE(2)–O>	**2.393**	**2.377**	**2.380**	**2.383**	**2.381**	**2.384**
Ca(3)/RE(3)–O(1)	2.222(20)	2.238 (9)	2.269(10)	2.258(8)	2.245(11)	2.216(9)
Ca(3)/RE(3)–O(2)						
Ca(3)/RE(3)–O(3)	2.267(15)	2.317 (7)	2.290(8)	2.307(7)	2.280(9)	2.278(8)
Ca(3)/RE(3)–O(3)	2.475(16)	2.476 (7)	2.463(8)	2.459(7)	2.453(10)	2.440(8)
Ca(3)/RE(3)–O(4)	2.207(15)	2.197 (7)	2.185(8)	2.202(7)	2.210(9)	2.196(8)
Ca(3)/RE(3)–O(4)	2.402(16)	2.419 (8)	2.445(8)	2.433(7)	2.414(10)	2.422(8)
Ca(3)/RE(3)–O(5)	2.304(18)	2.298(9)	2.332(9)	2.310(8)	2.271(11)	2.267(9)
Ca(3)/RE(3)–O(8)	2.327(17)	2.268(8)	2.297(8)	2.293(8)	2.292(10)	2.269(8)
Ca(3)/RE(3)–O(8)						
Ca(3)/RE(3)–O(10)						
<Ca(3)/RE(3)–O>	**2.315**	**2.316**	**2.326**	**2.323**	**2.309**	**2.298**
Bond angles						
Ge(1)–O(6)–Ge(2)	121.1(10)	120.7(4)	121.8(5)	122.5(4)	123.0(6)	123.3(5)
Ge(2)–O(9)–Ge(3)	125.5(10)	120.8(5)	123.2(5)	121.6(4)	121.9(6)	121.2(5)
Ge(1)–Ge(2)–Ge(3)	145.06(19)	144.60(8)	144.92(8)	144.84(7)	144.59(10)	144.71(8)
Specific distances						
A, Å	3.037	3.020	3.017	3.018	3.020	3.021
B, Å	2.926	2.924	2.925	2.916	2.910	2.903
C, Å	2.628	2.620	2.623	2.621	2.622	2.624
D, Å	0.313	0.316	0.309	0.308	0.325	0.325
E, Å	2.974	2.966	2.968	2.961	2.946	2.938

[a] The values of the distances between Ca and O(4) outside the first coordination sphere are given in *italics*.

[b] The bond valences calculated from the data by I. D. Brown and D. Altermatt.[40] The Ca(1)/RE(1)–O(4) distances and the corresponding bond valences have been calculated from the assumption of the first site to be occupied by only RE atoms.

Apart from the above, both transitions are accompanied by variation in the first and second coordination spheres of the Ca^{2+}/RE^{3+} cations (Tables 3 and 4; Fig. 5). Three Ca/RE sites have seven-fold coordination of oxygen atoms in the range from Yb to Gd, then the O(4) atom enters into the first coordination sphere. The Ca(1)/RE(1)–O(4) distances and the corresponding bond valences calculated from the assumption of the first site to be occupied by rare earths are included in Tables 3 and 4. In the Eu→Pr series, the distance decreases from 3.389(2) Å to 2.919(22) Å approaching to the average value of 2.554 Å calculated for $CaPr_2Ge_3O_{10}$. Bond valence contributed by O(4) grows from 0.021 to 0.121, respectively, so that the site m_1 has eight-fold coordination of oxygen atoms for $CaPr_2Ge_3O_{10}$. In the structure of $CaLa_2Ge_3O_{10}$, three Ca/La sites are coordinated by
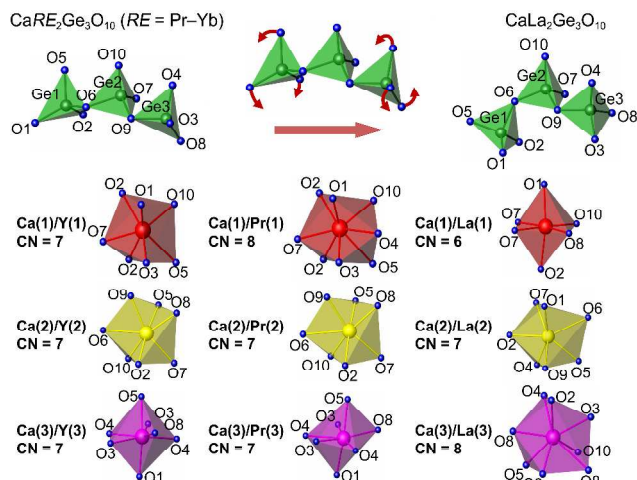
Fig. 5   The changes in the Ge_3O_{10} conformation and coordination environment of the three nonequivalent sites of metal cations within the structures of $CaRE_2Ge_3O_{10}$ (RE = Pr–Yb) and $CaLa_2Ge_3O_{10}$.

Fig. 6   The dependences of specific distances on average crystal radius in seven-fold coordination[38] for $CaRE_2Ge_3O_{10}$ (RE = Y, La–Yb).

six, seven and eight oxygen atoms, respectively, and the structural formula can be written as $(Ca_{0.93}La_{0.07})^{(VI)}(Ca_{0.07}La_{0.93})^{(VII)}(La_{1.00})^{(VIII)}Ge_3O_{10}$. Therefore, the change of the cation distribution, coordination numbers and geometry of Ge_3O_{10} with the average cation radius can explain both morphotropic transitions occurring between Gd–Eu and Pr–La, respectively. These transitions caused by the effects of local distortions and by significant variation of the crystal structure are also observed in $Ca_3Ln_2Ge_3O_{12}$ (Ln = Pr–Dy)[41] and $Ca_3Ln_2Si_3O_{12}$ (Ln = Eu–Lu)[42] with silico-carnotite structure, in catapleite-like $Sr_3Ln_2(Si_3O_9)_2$ (Ln = Eu–Lu),[5] as well as in the copper germanates $CuLn_2Ge_2O_8$ (Ln = La–Lu) and $CuLn_2Ge_4O_{12}$ (Ln = Eu–Lu) and silicates $CuLn_2Si_4O_{12}$ (Ln = Dy–Lu),[43] and other related compounds.

The calcium, germanium and rare earth atoms occupying the 4e sites have the following coordinates (x, y, z), (−x, y+1/2, −z+1/2), (−x, −y, −z), (x, −y+1/2, z+1/2). This means that every sort of atoms Ca(1)/RE(1), Ca(2)/RE(2), Ca(3)/RE(3), Ge(1), Ge(2), Ge(3) is located in its own plane which is perpendicular to the [0 0 1] direction and symmetrically relative to z = 0, ¼, ½, ¾ (Fig. 4). The specific distances represented in Tables 3, 4 and Fig. 4 show the crystal structure transformation. The distance A is an interval between the layers of the same type formed by Ca(1)/RE(1) and Ca(2)/RE(2) atoms; B is the distance between the layer with Ca(3)/RE(3) atoms and the nearest Ca(1)/RE(1) + Ca(2)/RE(2) layer; C is the space between the neighboring Ge(1) + Ge(2) layers; D is the thickness of layers consisting of Ge(3) atoms, and E is the distance between the Ge(3) and (Ge(1) + Ge(2)) layers. The dependences of the specific distances on the average crystal radius (CN = 7) are plotted in Fig. 6. While the values of A and B characterize the changes occurring in the layers of metal cations, the C, D and E distances reflect the variation of the geometry the Ge_3O_{10} unit. The thickness (D) of layers consisting of Ge(3) atoms is the most sensitive to the value of the average crystal radius with sevenfold coordination. Moreover, the A and D values show a well pronounced synchronous increase in the structures from the Yb to Pr compounds. However, the A distance decreases unlike to D in the lanthanum trigermanate.
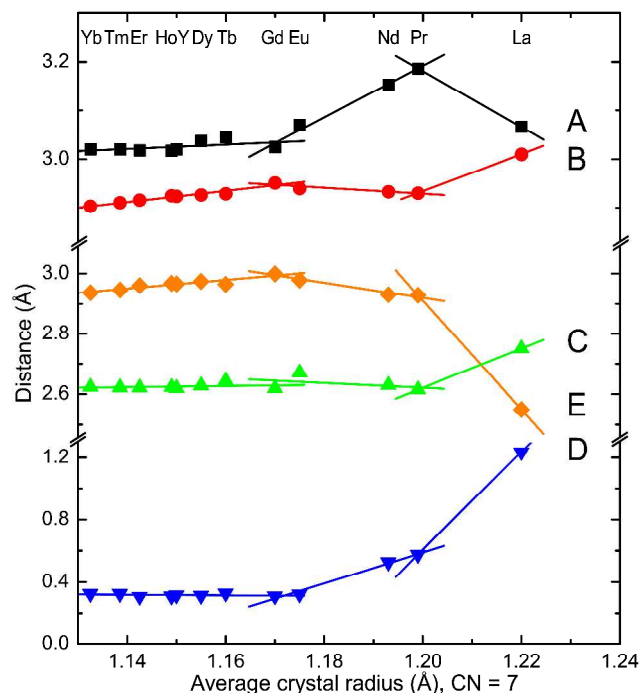
Meanwhile, A is more lanthanide ion-dependent than B as the former is associated directly with SOF of Ca(1)/RE(1) illustrated in Fig. 3. The behavior of the changes in the distances C and E is a similar to those in the couple of A and D as their values simultaneously vary in the crystal structures between the ytterbium and praseodymium compounds and change abruptly in $CaLa_2Ge_3O_{10}$ (Fig. 6). The Ge–Ge–Ge angle growth is accompanied by the straightening of Ge_3O_{10} and by the decrease of the monoclinic angle β. The tritetrahedral germanate group can be considered as a central tetrahedron $Ge(2)O_4$ and two terminal units $Ge(1)O_3$ and $Ge(3)O_3$. The parts $Ge(2)O_4 + Ge(1)O_3$ are the 'bridges' that connect the neighboring layers comprising the Ca(1)/RE(1) and Ca(2)/RE(2) atoms. The thickness of this block equals to A which is bound to the Ca(3)/RE(3) layer through $Ge(2)O_4 + Ge(3)O_3$. The above results demonstrate that $CaPr_2Ge_3O_{10}$ is the last member of the disordered germanates $CaRE_2Ge_3O_{10}$ (RE = Yb–Pr).

Vibrational spectroscopy

Four molecules of $CaRE_2Ge_3O_{10}$ (RE = Y, La–Yb) per primitive cell in the $P2_1/c$ (C_{2h}^5) structure support $3 \times 4 \times 16 = 192$ modes of vibration with K = 0 involving the zero-frequency translational motion of the crystal. These vibrations are classified according to irreducible representations of the point group of the elementary cell.[44] The 192 vibration modes of the full symmetry group result in the following irreducible representations of C_{2h}^5

$$\Gamma^{crys} = 48A_g + 48A_u + 48B_g + 48B_u, \qquad (2)$$

in view of all the atoms in the $CaRE_2Ge_3O_{10}$ cell occupy the 4e positions with $\Gamma = 3A_g + 3A_u + 3B_g + 3B_u$. Three of the unit cell phonons, $\Gamma^{acoust} = A_u + 2B_u$, describe the acoustic modes and the remaining ones,

$$\Gamma_{vib}^{cryst} = 48A_g + 47A_u + 48B_g + 46B_u, \qquad (3)$$

Table 5 Classification of the $k = 0$ unit cell modes^a for CaRE_2Ge$_3$O$_{10}$ (RE = Y, La–Yb); space group $P2_1/c$, $Z = 4$

Factor group	Lattice modes			Internal modes	Selection rules	
C_{2h}	Acoustic	Librational	Translational	[Ge$_3$O$_{10}$]$^{8-}$	infrared	Raman
A$_g$		3	12	33		$xx, yy, zz, xy,$
A$_u$	1	3	12	33	T_z	
B$_g$		3	12	33		$xz, yz,$
B$_u$	2	3	12	33	(T_x, T_y)	
Overall	3	12	48	132	$\sum = 192$	

^{a} The A$_u$ and B$_u$ modes are infrared and the combination of A$_g$ and B$_g$ is Raman active.
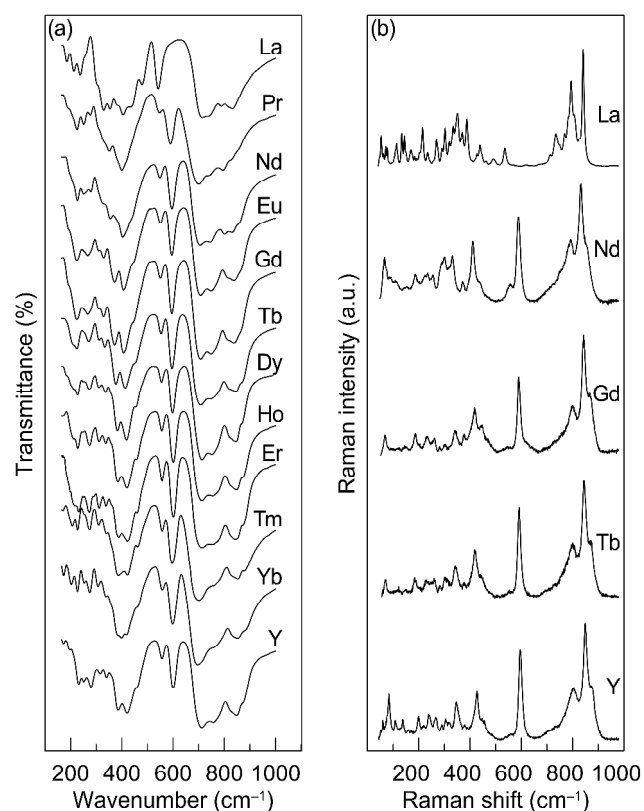
Fig. 7 (a) Infrared spectra of CaRE_2Ge$_3$O$_{10}$ (RE = Y, La–Yb). (b) Raman spectra of CaRE_2Ge$_3$O$_{10}$ (RE = Y, La, Nd, Gd and Tb).

correspond to the optical modes, among which there are no inactive ones. The modes of the A$_u$ and B$_u$ symmetry are infrared active and the other combination of A$_g$ and B$_g$ is Raman active.

The vibrational modes can be classified in two main categories, i.e. internal modes of the Ge$_3$O$_{10}$ unit with the molecular symmetry C_1 and external modes which include translations of the rare earth, calcium, and [Ge$_3$O$_{10}$]$^{8-}$ ions, and the [Ge$_3$O$_{10}$]$^{8-}$ librations. Infrared and Raman activity is represented in Table 5. Both translations and librations are associated by the same combinations

$$T'(\text{Ge}_3\text{O}_{10}) = L(\text{Ge}_3\text{O}_{10}) = 3A_g + 3A_u + 3B_g + 3B_u. \quad (4)$$

After the subtraction of acoustic modes, the external modes are distributed among the irreducible representation $15A_g + 14A_u + 15B_g + 13B_u$. Therefore, the internal modes of the tritetrahedral Ge$_3$O$_{10}$ unit are characterized by

$$\Gamma_{vib}^{int} = 33A_g + 33A_u + 33B_g + 33B_u. \quad (5)$$

They can be subdivided into three subgroups similarly to the triphosphate [P$_3$O$_{10}$]$^{5-}$ anion:[45] vibrations of the terminal GeO$_3$ groups and the GeOGe bridge bonds, and Ge$_3$O$_{10}$ deformations. The latter bears an analogy to ring vibrations in cyclotetragermanates.[46, 47] Moreover, the Ge$_3$O$_{10}$ group can be considered as a Ge$_2$O$_7$ pyrogroup connected with an additional GeO$_3$ unit. Thus, the stretching and bending movements of terminal GeO$_2$ in the central GeO$_4$ tetrahedron of Ge$_3$O$_{10}$ involve simultaneous motion of Ge atom relative to the bridge oxygen atom. The valence stretchings of the GeO$_3$ and GeOGe groups are identified in the usual way as symmetric (ν_s) and antisymmetric (ν_{as}) vibrations. Angular deformations are symbolized by δ and for deformations of the GeO$_3$ groups, in which the O–Ge–O angles are not modified the conventional notations are used for the rocking (ρ) and twisting (τ) modes.[45] Obviously, this classification is rather simple, because large mixing can occur when modes with the same symmetry are at about the same frequency that was earlier stressed by many authors.[44, 48, 49]

The polycrystalline FTIR and Raman spectra obtained for CaRE_2Ge$_3$O$_{10}$ (RE = Y, La–Yb) are shown in Fig. 7. The reliable Raman spectral data have been obtained only for the Y, La, Nd, Gd and Tb samples. Some rather strong luminescence artifacts under a 633 nm laser excitation have been found in the spectra of other lanthanide-containing compounds, and the Raman lines have been suppressed. The spectral contours in the full range are very complex. The spectra have not been deconvoluted into Lorentzian components as this fitting method had been criticized elsewhere and described as mathematic rather than crystallographic.[50] The absence of some predicted modes in the recorded spectra is attributed to degeneracy and/or low intensity of the corresponding bands. The low resolution of the lines in the Raman spectra of CaRE_2Ge$_3$O$_{10}$ (RE = Nd, Gd, Tb, Y) has also an instrumentation origin. A rather high transparency of submicroscale crystals and their imperfect form shown by scanning electron microscopy for a series of the CaRE_2Ge$_3$O$_{10}$ samples prepared by an EDTA-assisted route[35] do not allow precise focusing in the Raman microscopy experiment. Moreover, as the crystal structure of CaLa$_2$Ge$_3$O$_{10}$ is almost completely ordered unlike to CaRE_2Ge$_3$O$_{10}$ (RE = Yb–Pr) this may be the other reason of higher resolution of Raman lines in the CaLa$_2$Ge$_3$O$_{10}$ spectrum.

Whereas the molecular symmetry of the [Ge$_3$O$_{10}$]$^{8-}$ anion is C_1, the factor group is C_{2h}. According to the correlation diagram $C_1 \rightarrow C_{2h}$,[44] the internal vibrations have the form A$\rightarrow$A$_g$ + A$_u$ + B$_g$ + B$_u$ and for the [Ge$_3$O$_{10}$]$^{8-}$ free ion they can be distributed among:[45]

i) eight stretching modes of tetrahedral units – two ν_s(GeO$_3$)

and six $v_{as}(GeO_3)$,

ii) four stretching modes of the GeOGe bridges – two $v_s(GeOGe)$ and two $v_{as}(GeOGe)$,

iii) eight bending modes of the GeO_3 units – two $\delta_s(GeO_3)$ and six $\delta_{as}(GeO_3)$,

iv) other GeO_3 deformations – five $\rho(GeO_3)$ and three $\tau(GeO_3)$,

v) two bending modes of two GeOGe bonds – $\delta(GeOGe)$

vi) three Ge_3O_{10} deformations.

Stretching vibrations. In analogy with pyrogermanates, the $v_{as}(GeOGe)$ modes are expected to have the highest wavenumbers[51, 52] and appear as shoulders at ~860–890 cm^{-1} in the infrared spectra (Fig 6a). The most intensive Raman lines at 841; 833, 854; 843, 867; 845, 870; 849, 873 cm^{-1} in the spectra of $CaLa_2Ge_3O_{10}$, $CaNd_2Ge_3O_{10}$, $CaGd_2Ge_3O_{10}$, $CaTb_2Ge_3O_{10}$ and $CaY_2Ge_3O_{10}$, respectively, and infrared bands with middle intensity around 800–860 cm^{-1} ($CaRE_2Ge_3O_{10}$; RE = Y, La–Yb) can be assigned to the $v_s(GeO_3)$ modes.[51, 52] The other resolved ($CaLa_2Ge_3O_{10}$) and unresolved ($CaRE_2Ge_3O_{10}$, RE = Y, Nd, Gd, Tb) lines between 650 and 815 cm^{-1} are attributed to the antisymmetric GeO_3 strechings, which are also revealed as the most pronounced absorption bands at 630–800 cm^{-1} in the infrared counterparts. In the vibrational spectra of many isostructural series of lanthanide-containing antimonites, arsenates, germanates, phosphates and others, the bands are slightly displaced to higher wavenumbers with unit cell dimensions decreasing due to the phenomenon of lanthanide contraction.[46, 47, 53] However, only some of the vibrational bands in the high wavenumber interval in the spectra of $CaRE_2Ge_3O_{10}$ (RE = Gd–Yb) meet this tendency. The main reason is in the presence of the above considered morphotropic transitions occurring between the Gd–Eu and Pr–La compounds (Fig. 6). Meanwhile, a large vibration mixing of the $v_{as}(GeOGe)$ and $v_s(GeO_3)$ modes features many pyrogermanates.[51, 54, 55] In their turn, the $v_{as}(GeOGe)$ and $v_s(GeO_3)$ vibrations involve the motions of Ge atom in the central tetrahedron $Ge(2)O_4$ of the Ge_3O_{10} unit, which are found to be the most sensitive to variation of the Ge–O–Ge bond angle. The changes in Ge(1)–O(6)–Ge(2) and Ge(2)–O(9)–Ge(3) are different in three groups of trigermanates that is accompanied by the morphotropic transitions (Fig. 8).

The symmetric vibrations of the T–O–T bridges (T = Ge, Si) are known to be observed in the middle spectral range from 550 to 650 cm^{-1} in pyrogermanates and from 650 to 750 cm^{-1} in pyro- and trisilicates.[51, 52, 56] Meanwhile, the vibrations of the GeO_3 and GeOGe groups are either in-phase or out-of-phase that in its turn leads to the multiplicity of the IR bands and Raman lines predicted theoretically. Moreover, the opposed bridging oxygen atoms in the Ge_3O_{10} unit oscillate also in-phase or out-of-phase with respect to the neighboring one. This features also vibrational spectra of the silicates and germanates comprising the $[Si_3O_{10}]^{8-}$ and $[Ge_4O_{12}]^{8-}$ anions, respectively.[46, 47, 49, 56] The strong infrared band around 596 cm^{-1} and Raman line at ~590–596 cm^{-1} are assigned to the $v_s(GeOGe)$ vibrations in the spectra of $CaRE_2Ge_3O_{10}$ (RE = Nd, Gd, Tb, Y). However, the bands associated to $v_s(GeOGe)$ are shifted to 541 cm^{-1} and 536 cm^{-1} in the spectra of $CaLa_2Ge_3O_{10}$, and are represented as weak infrared band and Raman line, respectively (Fig. 7). Only weak shoulders at ~590 cm^{-1} (infrared spectrum) and ~570 cm^{-1} (Raman) remain
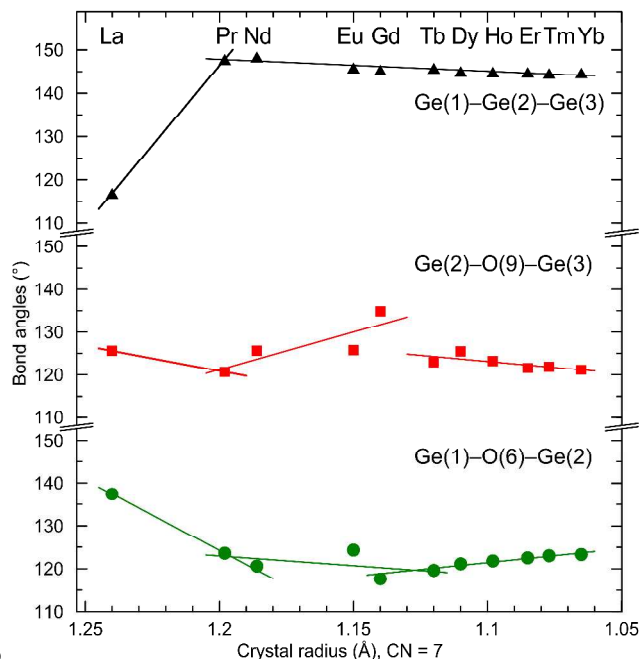
Fig. 8   The bond angles Ge(1)–O(6)–Ge(2), Ge(2)–O(9)–Ge(3) and Ge(1)–Ge(2)–Ge(3) depend on the crystal radius in seven-fold coordination[38] in the structure of $CaRE_2Ge_3O_{10}$ (RE = La–Yb). The values of crystal radii in seven-fold coordination estimated as mean values of radii in six- and eight-fold coordination are taken for Pr, Nd, Ho, Tm.

in the spectra of $CaLa_2Ge_3O_{10}$ near those positions of $v_s(GeOGe)$ from $CaRE_2Ge_3O_{10}$ (RE = Nd, Gd, Tb, Y). This stands in accordance with the evident angle distortion of Ge(1)–Ge(2)–Ge(3) illustrated in Figs. 5 and 8. While the symmetric GeOGe stretchings are not influenced by the deformation contribution in the spectra of germanates with the Ge_2O_7 pyrogroups,[51, 52, 55] this effect becomes apparent in vibration motions of the Ge_3O_{10} unit similar to Si_3O_{10} in silicates.[49, 56]

Bending vibrations. Bending motions of the terminal GeO_3 groups $\delta(GeO_3)$ contribute to the strong infrared absorption bands with shoulders and Raman lines between 360 and 570 cm^{-1}. However, other deformations of GeO_3, in which the O–Ge–O angles are not modified, i.e. $\rho(GeO_3)$ and $\tau(GeO3)$, arise in the low wavenumber limit of this range. The bending vibrations of the terminal Ge–O bonds reveal themselves more distinctly in infrared spectra than in Raman ones that is typical and stands also in line with the earlier studies of $Yb_2CuGe_4O_{12}$, Li_2TiGeO_5, $Sr_2ZnGe_2O_7$ and other pyrogermanates, and proves a strong vibrational mixing expected below ~550 cm^{-1}.[46, 51, 55, 57]

Vibrations in the region of lattice modes. A part of the region of lattice modes is out of our infrared instrument range. In the Raman spectrum no peaks lower than 50 cm^{-1} have been observed. Experimental spectra below 520 cm^{-1} appear rather complex and the assignment in this wavenumber range is not unequivocal. Some of the infrared bands in the range 280–475 cm^{-1} are assigned to the T′(Ca) and T′(RE) translations which involve the motions of the Ge_3O_{10} sub-lattice and overlap with ρ and τ modes of the GeO_3 groups, and bending vibrations of the GeOGe bridges revealed more clearly in the Raman spectrum. The latter features also vibrational spectra of some pyro- and

cyclotetragermanates with isolated Ge_2O_7 and Ge_4O_{12} units in the crystal structure, respectively.[46, 47, 51, 55] The modes in the range $0–280$ cm^{-1} are related to the Ge_3O_{10} deformations, translational motions of metal cations as well as to translations and librations of the Ge_3O_{10} unit that are difficult to decouple. The character of representation for the Ge_3O_{10} librational modes in $CaRE_2Ge_3O_{10}$, RE = Y, La–Yb, (the factor group C_{2h} and molecular symmetry C_1) is the same as for translations of Ge_3O_{10} (Eq. 4). Therefore, a strong vibrational mixing between these two groups of modes is expected, that is usually revealed in crystals with low symmetry.[44] Some of the observed Raman lines located at $50–220$ cm^{-1} correspond to the Ge_3O_{10} librations. The latter are usually associated with large changes in polarizability and translational modes originate from large dipole moment changes. As a result librational modes give usually rise to relatively intense Raman and weak infrared bands whereas the opposite behavior is expected for the translational modes.[58] However, the relative intensity of the Raman lines and infrared bands is rather similar in the low wavenumber region in the case of $CaRE_2Ge_3O_{10}$ (RE = Y, La–Yb) that also evidences the mixing between the Ge_3O_{10} translations and librations predicted theoretically. Meanwhile, the inspection of the recorded spectra shows the presence of Raman lines with middle intensity in the $50–220$ cm^{-1} range, which are most likely assigned to vibrations involving large contribution of the Ge_3O_{10} librations.

Conclusion

The performed powder XRD study has shown that $CaRE_2Ge_3O_{10}$ (RE = Y, La–Yb) crystallize in the monoclinic system with the space group $P2_1/c$, $Z = 4$. The lattice parameters and volumes follow the linear dependence on the crystal radius of RE^{3+} until two morphotropic transitions. The first transition between Eu and Gd compounds results in change of direction of the unit cell parameters dependence vs. crystal radius of rare earth without any anomaly of unit cell volume, and the second transition between Pr and La has a step-like change of all the unit cell parameters including the volume.

The calcium and rare earth fractions have been found to change from mixed in $CaRE_2Ge_3O_{10}$ (RE = Y, Pr–Yb) to ordered in $CaLa_2Ge_3O_{10}$. The variation of the rare earth radius leads to a change of the cations' layer thickness, which results in a variation of the Ge_3O_{10} geometry. In the first group of compounds ($CaYb_2Ge_3O_{10}$–$CaPr_2Ge_3O_{10}$) the angle Ge–Ge–Ge increases from 144.7° (Yb) to 148.4° (Pr), but in the case of $CaLa_2Ge_3O_{10}$ this angel becomes equal to 116.2° and the conformation changes. All these lead to the variation in the first and second coordination spheres of Ca^{2+}/RE^{3+}. One should expect similar polymorphic transitions in this series with temperature and pressure, which are analogous to chemical lattice expansion caused by increasing cation size from Yb–Gd to Eu–Pr and to La.

Acknowledgements

Notes and references

^{a} Institute of Solid State Chemistry, UB RAS, 620990 Ekaterinburg, Russia. Fax: +7 343 374 44 95; E-mail: ivanleonidov@ihim.uran.ru
^{b} Ural Federal University, 620002 Ekaterinburg, Russia
^{c} Institute of High-Temperature Electrochemistry, UB RAS, 620990 Ekaterinburg, Russia
† Electronic Supplementary Information (ESI) available: details of Rietveld refinement of room temperature powder X-ray diffraction patterns (Figs. S1–S12), atomic coordinates, isotropic thermal parameters and Ca^{2+}–RE^{3+} fractions in the structures of $CaRE_2Ge_3O_{10}$; RE = Y, La–Yb (Tables S1–S4). See DOI: 10.1039/b000000x/

1 (a) G. Blasse, W. L. Wanmaker, J. W. ter Vrugt and A. Bril, *Philips Res. Rep.*, 1968, **23**, 189–200; (b) I. A. Bondar, A. A. Kolpakova, L. Ya. Markovskii, A. N. Sokolov, L. E. Tarasova and N.A. Toropov, *Izv. Akad. Nauk SSSR, Ser. Fiz.*, 1969, **33**, 1057.

2 M. S. Wickleder, *Chem. Rev.*, 2002, **102**, 2011–2087.

3 (a) H. A. Hoppe, *Angew. Chem. Int. Ed.*, 2009, **48**, 3572–3582; (b) S. Ye, F. Xiao, Y. X. Pan, Y. Y. Ma and Q. Y. Zhang, *Mater. Sci. Eng. R–Rep.*, 2010, **71**, 1–34.

4 (a) K. I. Machida, G. Y. Adachi, J. Shiokawa, M. Shimada, M. Koizumi, K. Suito and A. Onodera, *Inorg. Chem.*, 1982, **21**, 1512–1519; (b) S. H. M. Poort, H. M. Reijnhoudt, H. G. T. van der Kuip and G. Blasse, *J. Alloys Compd.*, 1996, **241**, 75–81 and references therein; (c) S. H. M. Poort, A. Meijerink and G. Blasse, *J. Phys. Chem. Solids*, 1997, **58**, 1451–1456; (d) T. Nagasawa, H. Yamane, S. Kubota and M. Shimada, *J. Ceram. Soc. Jpn.*, 1998, **106**, 1238–1241 and references therein; (e) Z. G. Cui, G. H. Jia, D. G. Deng, Y. J. Hua, S. L. Zhao, L. H. Huang, H. P. Wang, H. P. Ma and S. Q. Xu, *J. Lumin.*, 2012, **132**, 153–160; (f) H. K. Yang, H. M. Noh, B. K. Moon, J. H. Jeong and S. S. Yi, *Ceram. Int.*, 2014, **40**, 12503–12508.

5 A. P. Tyutyunnik, I. I. Leonidov, I. F. Berger, L. L. Surat and V. G. Zubkov, *J. Solid State Chem.*, 2013, **197**, 447–455 and references therein.

6 (a) V. R. Bandi, Y. T. Nien, T. H. Lu and I. G. Chen, *J. Am. Ceram. Soc.*, 2009, **92**, 2953–2956; (b) V. R. Bandi, Y. T. Nien and I. G. Chen, *J. Appl. Phys.*, 2010, **108**, 023111; (c) V. R. Bandi, B. K. Grandhe, K. Jang, H. S. Lee, S. S. Yi and J. H. Jeong, *Ceram. Int.*, 2011, **37**, 2001–2005.

7 (a) F. Piccinelli, A. Speghini, G. Mariotto, L. Bovo and M. Bettinelli, *J. Rare Earths*, 2009, **27**, 555–559; (b) K. V. Ivanovskikh, A. Meijerink, F. Piccinelli, A. Speghini, E. I. Zinin, C. Ronda and M. Bettinelli, *J. Lumin.*, 2010, **130**, 893–901.

8 (a) B. V. Rao, Y. T. Nien, W. S. Hwang and I. G. Chen, *J. Electrochem. Soc.*, 2009, **156**, J338–J341; (b) Z. J. Zhang, A. C. A. Delsing, P. H. L. Notten, J. T. Zhao and H. T. Hintzen, *Mater. Res. Bull.*, 2012, **47**, 2040–2044.

9 (a) Y. Wen, Y. H. Wang, F. Zhang and B. T. Liu, *Mater. Chem. Phys.*, 2011, **129**, 1171–1175; (b) Y. Wen, Y. H. Wang, B. T. Liu and F. Zhang, *Opt. Mater.*, 2012, **34**, 889–892.

10 (a) J. Lin and Q. Su, *J. Mater. Chem.*, 1995, **5**, 603–606; (b) X. M. Han, J. Lin, Z. Li, X. W. Qi, M. Y. Li and X. Q. Wang, *J. Rare Earths*, 2008, **26**, 443–445; (c) G. G. Li, Y. Zhang, D. L. Geng, M. M. Shang, C. Peng, Z. Y. Cheng and J. Lin, *ACS Appl. Mater. Interfaces*, 2012, **4**, 296–305.

11 (a) A. Dobrowolska and E. Zych, *J. Solid State Chem.*, 2011, **184**, 1707–1714; (b) Z. P. Yang, X. S. Liang, Y. H. Zhao, C. C. Hou, C. Wang and H. Y. Dong, *J. Chin. Ceram. Soc.*, 2013, **41**, 1720–1724; (c) Z. P. Yang, H. Y. Dong, X. S. Liang, C. C.

Hou, L. P. Liu and F. C. Lu, *Dalton Trans.*, 2014, **43**, 11474–11477.

12 (*a*) Y. C. Chiu, W. R. Liu, Y. T. Yeh, S. M. Jang and T. M. Chen, *J. Electrochem. Soc.*, 2009, **156**, J221–J225; (*b*) Y. C. Chiu, W. R. Liu, Y. T. Yeh, S. M. Jang and T. M. Chen. *ECS Transactions*, 2009, **25**, 157–165; (*c*) N. X. Li, S. Q. Li, Y. M. Wang, B. Y. Zhou, Y. M. Sun and J. C. Zhou, *J. Rare Earths*, 2014, **32**, 933–937; (*d*) M. Müller and Th. Jüstel, *J. Lumin.*, 2014, **155**, 398–404.

13 H. S. Jang and D. Y. Jeon, *Appl.Phys. Lett.*, 2007, **90**, 041906.

14 M. P. Saradhi and U. V. Varadaraju, *Chem.Mater.*, 2006, **18**, 5267–5272.

15 D. Y. Wang, C. H. Huang, Y. C. Wu and T. M. Chen, *J. Mater. Chem.*, 2011, **21**, 10818–10822.

16 H. D. Ju, B. L. Wang, Y. H. Ma, S. B. Chen, H. Wang and S. Yang, *Ceram. Int.*, 2014, **40**, 11085–11088.

17 (*a*) S. Ray, Y. C. Fang and T. M. Chen, *RSC Adv.*, 2013, **3**, 16387–16391; (*b*) G. Zhu, Y. R. Shi, M. Mikami, Y. Shimomura and Y. H. Wang, *CrystEngComm*, 2014, **16**, 6089–6097.

18 C. H. Huang and T. M. Chen, *Inorg. Chem.*, 2011, **50**, 5725–5730.

19 M. F. Zhang, Y. J. Liang, Rui Tang, D. Y. Yu, M. H. Tong, Q. A. Wang, Y. L. Zhu, X. Y. Wu and G. G. Li, *RSC Adv.*, 2014, **4**, 40626–40637.

20 (*a*) Y. L. Liu, B. F. Lei and C. H. Shi, *Chem. Mater.*, 2005, **17**, 2108–2113; (*b*) Y. L. Liu, J. Y. Kuang, B. F. Lei and C. H. Shi, *J. Mater. Chem.*, 2005, **15**, 4025–4031.

21 (*a*) L. C. V. Rodrigues, H. F. Brito, J. Hölsä, R. Stefani, M. C. F. C. Felinto, M. Lastusaari, T. Laamanen and L. A. O. Nunes, *J. Phys. Chem. C*, 2012, **116**, 11232−11240; (*b*) L. C. V. Rodrigues, J. Hölsä, M. Lastusaari, M. C. F. C. Felinto and H. F. Brito, *J. Mater. Chem. C*, 2014, **2**, 1612–1618.

22 (*a*) T. Aitasalo, J. Hölsä, M. Lastusaari, J. Legendziewicz, J. Niittykoski and F. Pellé, *Opt. Mater.*, 2004, **26**, 107–112; (*b*) P. Dorenbos, C. W. E. van Eijk, A. J. J. Bos, C. L. Melcher, *J. Phys.: Condens.Matter*, 1994, **6**, 4167–4180.

23 (*a*) Y. Lin, Z. Tang, Z. Zhang, X. Wang, J. Zhang, *J. Mater. Sci. Lett.*, 2001, **20**, 1505–1506; (*b*) T. Aitasalo, J. Hölsä, T. Laamanen, M. Lastusaari, L. Lehto, J. Niittykoski and F. Pellé, *Ceram.–Silikáty*, 2005, **49**, 58–62.

24 (*a*) K. Van den Eeckhout, P. F. Smet and D. Poelman, *Materials*, 2010, **3**, 2536–2566; (*b*) K. Van den Eeckhout, D. Poelman and P. F. Smet, *Materials*, 2013, **6**, 2789–2818.

25 (*a*) K. Takagi and T. Fukazawa, *Appl. Phys.Lett.*, 1983, **42**, 43–45; (*b*) C. L. Melcher and J. S. Schweitzer, *Nucl. Instrum. Methods Phys. Res., Sect. A.*, 1992, **314**, 212–214; (*c*) B. Chai and Y.Ji, *US Pat.*, 6 624 420, 2000; (*d*) V. Jary, M. Nikl, G. Ren, P. Horodysky, G.P. Pazzi and R. Kucerkova, *Opt. Mater.*, 2011, **34**, 428–432; (*e*) O. Sidletskiy, A. Belsky, A. Gektin, S. Neicheva, D. Kurtsev, V. Kononets, C. Dujardin, K. Lebbou, O. Zelenskaya, V. Tarasov, K. Belikov and B. Grinyov, *Cryst. Growth Des.*, 2012, **12**, 4411−4416; (*f*) V. Jarý, E. Mihóková, J. A. Mareš, A. Beitlerová, D. Kurtsev, O. Sidletskiy and M. Nikl, *J. Phys. D: Appl. Phys.*, 2014, **47**, 365304.

26 J. Pejchal, M. Nikl, E. Mihóková, J. A. Mareš, A. Yoshikawa, H. Ogino, K. M. Schillemat, A. Krasnikov, A. Vedda, K. Nejezchleb and V. Múčka, *J. Phys. D: Appl. Phys.*, 2009, **42**, 055117.

27 (*a*) L. Pidol, A. Kahn-Harari, B. Viana, B. Ferrand, P. Dorenbos, J. T. M. de Haas, C. W. E. van Eijk and E. Virey, *J. Phys.: Condens. Matter*, 2003, **15**, 2091–2102; (*b*) O. Sidletskiy, V. Baumer, I. Gerasymov, B. Grinyov, K. Katrunov, N. Starzhinsky, O. Tarasenko, V. Tarasov, S. Tkachenko, O. Voloshina and O. Zelenskaya, *Radiat. Meas.*, 2010, **45**, 365–368; (*c*) A. Suzuki, S. Kurosawa, T. Shishido, J. Pejchal, Y. Yokota, Y. Futami and A. Yoshikawa, *Appl. Phys. Express*, 2012, **5**, 102601; (*d*) Q. H. Wei, G. H. Liu, Z. Z. Zhou, J. Q. Wan, H. Yang and Q. Liu, *Mater. Lett.*, 2014, **126**, 178–180.

28 K. V. Ivanovskikh, A. Meijerink, F. Piccinelli, A. Speghini, C. Ronda and M. Bettinelli, *ECS J. Solid State Sci. Technol.*, 2012, **1**, R127-R130.

29 U. Kolitsch, M. Wierzbicka and E. Tillmanns, *Acta Crystallogr. Sect. C-Cryst. Struct. Commun.*, 2006, **62**, i97–i99.

30 W. R. Liu, C. C. Lin, Y. C. Chiu, Y. T. Yeh, S. M. Jang, R. S. Liu and B. M. Cheng, *Opt. Express*, 2009, **17**, 18103–18109.

31 (*a*) Z. G. Xia, Y.J. Liang, D. Y. Yu, M. F. Zhang, W. Z. Huang, M. H. Tong, J. M. Wu and J. W. Zhao, *Optics & Laser Technol.*, 2014, **56**, 387–392; (*b*) J. Q. Wang, W. R. Zhao, J. M. Zhong and L. C. Lan, *J. Mater. Sci.–Mater. Electron.*, 2014, **25**, 2162–2168.

32 (*a*) M. Wierzbicka-Wieczorek, U. Kolitsch and E. Tillmanns, *Eur. J. Mineral.*, 2010, **22**, 245–258; (*b*) M. Wierzbicka-Wieczorek, C. Lenz and G. Giester, *Eur. J. Inorg. Chem.*, 2013, 3405–3411.

33 H. Yamane, R. Tanimura, T. Yamada, J. Takahashi, T. Kajiwara and M. Shimada, *J. Solid State Chem.*, 2006, **179**, 289–295.

34 (*a*) Yu. I. Smolin, Yu. F. Shepelev and T. V. Upatova, *Dokl. Akad. Nauk SSSR*, 1969, **187**, 322–325; (*b*) B. A. Maksimov, V. V. Ilyukhin and N. V. Belov, *Sov. Phys. Dokl.*, 1978, **23**, 699; (*c*) G. Vetter and F. Queroux, *J. Solid State Chem.*, 1988, **73**, 287–297; (*d*) C. Linke and M. Jansen, *Z. Naturforsch., B: Chem. Sci.*, 1996, **51**, 1591–1597.

35 (*a*) O. A. Lipina, L. L. Surat, M. A. Melkozerova, A. P. Tyutyunnik, I. I. Leonidov and V. G. Zubkov, *J. Solid State Chem.*, 2013, **206**, 117–121; (*b*) O. A. Lipina, L. L. Surat, M. A. Melkozerova, A. P. Tyutyunnik, I. I. Leonidov and V. G. Zubkov, *Opt. Spectrosc.*, 2014, **116**, 695–699.

36 (*a*) B. H. Toby, *J. Appl. Crystallogr.*, 2001, **34**, 210–213; (*b*) A. C. Larson and R. B. Von Dreele, General Structure Analysis System (GSAS), Los Alamos National Laboratory Report LAUR 86–748, Los Alamos, NM (2004).

37 A. Altomare, C. Cuocci, C. Giacovazzo, A. Moliterni, R. Rizzi, N. Corriero and A. Falcicchio, *J. Appl. Crystallogr.*, 2013, **46**, 1231–1235.

38 R. D. Shannon, *Acta Crystallogr. Sect. A*, 1976, **32**, 751–767.

39 (*a*) J. B. Clark, J. W. Hastie, L. H. E. Kihlborg, R. Metselaar and M. M. Thackeray, *Pure Appl. Chem.*, 1994, **66**, 577–594; (*b*) J. C. Tolédano, R. S. Berry, P. J. Brown, A. M. Glazer, R. Metselaar, D. Pandey, J. M. Perez-Mato, R. S. Roth and S. C. Abrahams, *Acta Crystallogr. Sect. A*, 2001, **57**, 614–626.

40 I. D. Brown and D. Altermatt, *Acta Crystallogr. Sect. B*, 1985, **41**, 244–247.

41 F. Piccinelli, A. Lausi and M. Bettinelli, *J. Solid State Chem.*, 2013, **205**, 190–196.

42 F. Piccinelli, A.Lausi, A.Speghini and M.Bettinelli, *J. Solid State Chem.*, 2012, **194**, 233–237.

43 U. Lambert and W. Eysel, *Powder Diffr.*, 1986, **1**, 256–260.

44 (*a*) W. G. Fateley, N. T. McDevitt and F. F. Bentley, *Appl. Spectrosc.*, 1971, **25**, 155–173; (*b*) D. L. Rousseau, R. P. Bauman and S. P. S. Porto, *J. Raman Spectrosc.*, 1981, **10**, 253–290.

45 W. Bues and H. W. Gehrke, *Z. Anorg. Allg. Chem.*, 1956, **288**, 291–306.

46 E. J. Baran, C. C. Wagner, A. E. Lavat and C. Cascales, *J. Raman Spectrosc.*, 1997, **28**, 927–931.

47 I. I. Leonidov, V. P. Petrov, V. A. Chernyshev, A. E. Nikiforov, E. G. Vovkotrub, A. P. Tyutyunnik and V. G. Zubkov, *J. Phys. Chem. C*, 2014, **118**, 8090−8101.

48 (*a*) P. Tarte, M. J. Pottier and A. M. Procès, *Spectrochim. Acta, Part A*, 1973, **29**, 1017–1027; (*b*) Y. Noël, M. Catti, Ph. D'Arco and R. Dovesi, *Phys. Chem. Miner.*, 2006, **33**, 383–393.

49 R. Kaindl, D. M. Többens and V. Kahlenberg, *J. Raman Spectrosc.*, 2011, **42**, 78–85.

50 (*a*) T. S. Hammink, W. T. Fu and D. J. W. Ijdo, *J. Solid State Chem.*, 2011, **184**, 848–851; (*b*) W. Y. Li, L. X. Ning and P. A. Tanner, *J. Phys. Chem. A*, 2012, **116**, 7337−7344.

51 M. Gabelica-Robert and P. Tarte, *Spectrochim. Acta, Part A*, 1979, **35**, 649–654.

52 R. Saez-Puche, M. Bijkerk, F. Fernández, E. J. Baran and I. L. Botto, *J. Alloys Compd.*, 1992, **184**, 25–34.

53 (*a*) K. P. F. Siqueira, P. P. Lima, R. A. S. Ferreira, L. D. Carlos, E. M. Bittar, E. Granado, J. C. González, A. Abelenda, R. L. Moreira and A. Dias, *Chem. Mater.*, 2014, **26**, 6351–6360; (*b*) A. E. Lavat, M. Trezza, I. L. Botto, D. I. Roncaglia and E. J. Baran, *Spectrosc. Lett.*, 1988, **21**, 355–366; (*c*) E. J. Baran and C. Cascales, *J. Raman Spectrosc.*, 1999, **30**, 77–79.

54 A. N. Lazarev, *Vibrational Spectra and Structure of Silicates*, Consultants Bureau, New York, 1972.

55 J. Hanuza, M. Mączka, M. Ptak, J. Lorenc, K. Hermanowicz, P. Becker, L. Bohatý and A. A. Kaminskii, *J. Raman Spectrosc.*, 2011, **42**, 782–789.

56 M. Wierzbicka-Wieczorek, D. M. Többens, U. Kolitsch and E. Tillmanns, *J. Solid State Chem.*, 2013, **207**, 94–104.

57 M. Mączka, A. Sieradzki, R. Poprawski, K. Hermanowicz and J. Hanuza, *J. Phys.: Condens. Matter*, 2006, **18**, 2137–2147.

58 P. E. Tomaszewski, M. Mączka, A. Majchrowski, A. Waśkowska and J. Hanuza, *Solid State Sci.*, 2005, **7**, 1201–1208.

This journal is © The Royal Society of Chemistry [year]
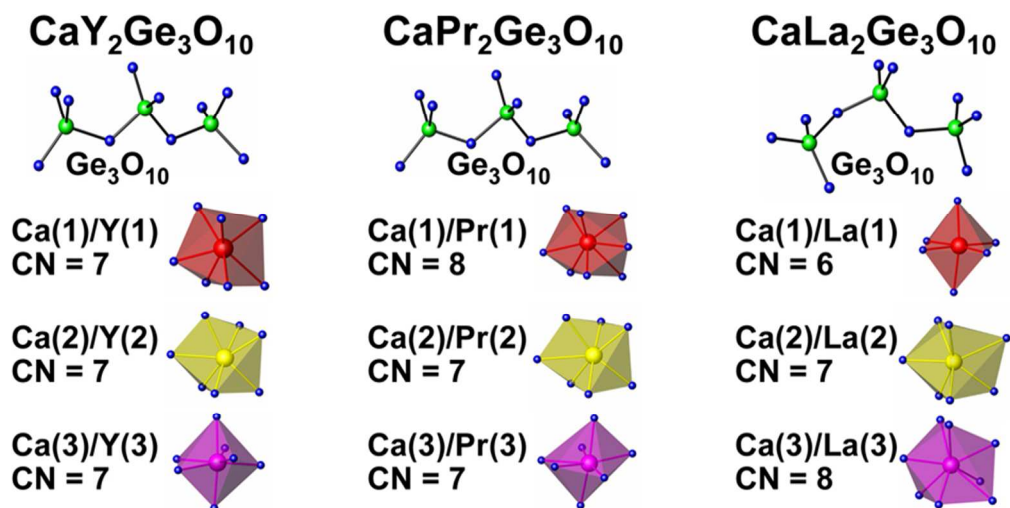
Graphical abstract. The changes in the Ge_3O_{10} conformation and coordination environment of the three non-equivalent cations within the structures of $CaY_2Ge_3O_{10}$, $CaPr_2Ge_3O_{10}$ and $CaLa_2Ge_3O_{10}$.

80x39mm (300 x 300 DPI)